physica status solidi

pss

www.pss-journals.com

reprint

WILEY-VCH

Phys. Status Solidi B **252**, No. 6, 1402–1409 (2015) / **DOI** 10.1002/pssb.201451657

physica status solidi b
www.pss-b.com
basic solid state physics

Magnetoresistance and electrical resistivity of N-doped multi-walled carbon nanotubes at low temperatures

I. V. Ovsienko[1], T. A. Len[1], L. Yu. Matsuy[1], Yu. I. Prylutskyy[1], I. B. Berkutov[*,2], V. V. Andrievskii[2], Yu. F. Komnik[2], I. G. Mirzoiev[2], G. E. Grechnev[2], Yu. A. Kolesnichenko[2], R. Hayn[3], and P. Scharff[4]

[1] Taras Shevchenko National University of Kyiv, 64 Volodymyrska Str., 01601 Kyiv, Ukraine
[2] B. Verkin Institute for Low Temperature Physics and Engineering of the National Academy of Sciences of Ukraine, 47 Lenin Ave., 61103 Kharkov, Ukraine
[3] Universite d'Aix-Marseille, IM2NP, 13397 Marseille Cedex 20, France
[4] Technical University of Ilmenau, Weimarer Str. 25, 98683 Ilmenau, Germany

Received 4 November 2014, revised 28 December 2014, accepted 21 January 2015
Published online 4 March 2015

Keywords carbon nanotubes, magnetoresistance, nitrogen doping, phase relaxation times, resistivity, weak localizations

[*] Corresponding author: e-mail berkutov@ilt.kharkov.ua, Phone: +380-57-340-22-23, Fax: +380-57-3410963

The magnetoresistance and electrical resistivity of nitrogen-doped multi-walled carbon nanotubes (N-MWCNTs) were studied in the temperature range of 1.6–100.3 and 1.6–286 K, respectively, using a standard four-probe technique. The possible mechanisms of the observed effects are discussed in detail.

1 Introduction Carbon nanotubes (CNTs) exhibit unique chemical and physical properties that allow employing them in a variety of applications. In particular, CNTs are chemically and thermally stable, characterized by high mechanical strength, thermal and electrical conductivity, and large specific surface area. Currently, CNTs are regarded as the most attractive building blocks for nanoelectronics, since they are able to form an almost perfect spin-transport medium. Basically, the electron transport in them is one-dimensional and ballistic with a long spin relaxation time and weak spin–orbit effects. Also, even pristine CNTs, which are non-magnetic materials, are characterized by a giant magnetoresistance [1]. On the other hand, it is quite obvious that modification of CNTs (intercalation and filling the internal cavities with different elements) can lead to significant differences in their electronic structure and physical properties [2–5].

One of the possible types of CNT modification is substitution of the carbon atoms by atoms of other elements, in particular by boron or nitrogen. The substitution of the carbon atoms can be realized using atoms of the same type or by the atoms of different type simultaneously. Such substitution gives the possibility to create new types of nanomaterials with different properties and also opens up new opportunities for application of CNTs to electronic devices. It is well known that nitrogen (N) doping of CNTs creates an electron donor state in the conduction band near the Fermi level [6]. At the same time, boron doping of CNTs led to the increase of the density of acceptor states near the valence band edge. As shown in the series of papers [7–12], the nitrogen doping of CNTs provides significant changes in morphology, hardness and chemical reactivity. The theoretical aspects of the influence of doping on the electronic structure and kinetic properties of CNT were studied in Refs. [13–15]. In Ref. [13] the shift of the Fermi level in doped CNT was analyzed as a function of the nitrogen or boron concentration. It was shown (see Ref. [15] for details) that N-doped CNTs exhibit metallic properties independently of their chirality. At the same time, experimental investigations of the kinetic properties of doped CNTs do not provide a consistent view on the origin of those properties. In Ref. [16], it was found that the thermal electromotive force of N-doped multi-walled carbon nanotubes (MWCNTs) is of an opposite sign. This is evidence that the type of main carriers changes as a result

of the modification of MWCNT by nitrogen. The thermal electromotive force was analyzed in the framework of the model of strong localization of charge carriers, which adequately describes the charge transport in disordered carbon systems and noncrystalline semiconductors. This model was used to describe the conductivity of K-doped CNT fibers in Ref. [17]. In Ref. [18], the magnetoresistance and thermal electromotive force of I-doped CNT was analyzed in the framework of the weak localization model for 3D systems. The highest concentration of nitrogen has been obtained when nitrogen was incorporated in MWCNTs, namely N content >20% with respect to carbon [19]. However, despite the great attention devoted to the doped systems in general, and to N-MWCNTs in particular [20–25], the understanding of the relationship between the structure and the kinetic properties of this nanosystem is one of the most fundamental problems in material science.

Thus, the goal of this work is to study the magnetoresistance and electrical resistivity of N-doped MWCNT at low temperatures, and to analyze in detail their possible mechanisms.

2 Experimental Undoped and N-doped MWCNT were grown on the walls of a quartz tube reactor using a spray pyrolysis CVD method. Argon as a carrier gas was used under a pressure of 20 kPa. Benzene (BZ) and acetonitrile (ACN) containing $FeCp_2$ (2%) were applied as feedstock materials for the synthesis of undoped and N-doped MWCNT. The experimental setup for CNT growth is described in detail in Ref. [26].

For measurements of electrical resistivity and magnetoresistance of CNT, the compacted samples were prepared by cold pressing using a polyvinyl acetate adhesive (85 wt% pristine or N-MWCNT, 15 wt% polyvinyl acetate). The density of obtained compacted samples was 1.38 g cm^{-3} for nondoped CNTs and 1.40 g cm^{-3} for doped CNTs. Magnetoresistance and resistivity of samples were investigated in the temperature ranges 1.6–100.3 and 1.6–286 K, respectively, using a standard four-probe technique. The magnetic field induction up to 5 T was applied perpendicular to the direction of the electric current.

3 Results and discussion The detailed structure characterization of the obtained materials by scanning electron microscopy (SEM; FEI XL30 LaB_6) in Fig. 1a from Ref. [24], high-resolution transmission electron microscopy (HRTEM) in Fig. 1b from Ref. [24], X-ray diffraction spectroscopy (XRD), in Fig. 2 from Ref. [24], are presented in Refs. [24, 26]. SEM images obtained from the deposited films exhibit essential differences in the morphology of undoped and N-doped MWCNT [24, 26]. N-doped MWCNTs are smoother than pure MWCNTs. According to the high-resolution electron microscopic images the obtained N-MWCNT show bamboo-like structure of nanotubes result from nitrogen doping, since nitrogen plays a key role in generating compartment layers inside the nanotubes. The inner diameter of N-MWCNT is between 30 and 40 nm, whereas the outer diameter ranges from 50 to 100 nm and the length is up to 15 μm. The structure of undoped MWCNTs differs notably. The nanotubes have an outer average diameter of about 30 nm and are usually composed of concentric cylinders rather than bamboo-like segments. The diameter of the central channel varies from 5 to 20 nm. The XRD pattern of N-MWCNT grown with decomposition of ACN exhibits weak peaks that could be ascribed to the hexagonal C_3N_4 (201) and (004) reflections [26]. These features prove the quite homogeneous distribution of N atoms in the CNT grown with decomposition of ACN [24, 26]. Incorporation of nitrogen into CNT is also confirmed by Raman spectra investigations. A slight up-shifting of the G-band position, the change of I_D/I_G ratio in the N-doped CNTs in comparison with n-doped CNT, and the decreasing of the D* band relative intensity indicate that nitrogen is incorporated in the tubule walls [26]. The chemical composition of the NTs arrays determined with an energy dispersive X-ray spectrometer is 92.6 at.% of carbon, 7 at.% of nitrogen and 0.4 at.% of iron [26].

Figure 1 shows the temperature dependence of the resistivity $\rho(T)$ for the pure MWCNT and N-MWCNT samples in the temperature range of 1.6–286 K. A decrease in resistance with increasing temperature took place for both pure MWCNT and N-MWCNT samples. However, in the entire temperature range the resistance of nitrated MWCNT is about six times less than the resistance of pure MWCNT. This indicates the increase of the number of free charge carriers in MWCNT in a nitrogen-doping process. At temperatures >40 K for the pure MWCNT (Fig. 1a) and >20 K for the nitrated MWCNT (Fig. 1b) a weak monotonic decrease of the specific electric resistance is observed. Such a weak temperature dependence of the electric resistance was explained by features of the charge-carrier scattering in graphite-based materials and particularly in MWCNT [27]. As is known, the electronic structure of MWCNT with a large number of graphite layers similar to the electronic structure of the fine-crystalline graphites. Therefore, the analysis of the conductivity of such MWCNT can be carried out in the framework of Wallace's model [28], which is used to describe the conductivity of slightly ordered fine-crystalline graphites. Taking into account the classic mechanisms of charge-carrier scattering within this model the electric resistance can be written as:

$$\rho = \frac{\pi \sqrt{3}\, \gamma_0\, a_0\, d_{002}\, \hbar}{\Delta E_F\, e^2 L_{ef}}, \tag{1}$$

where γ_0 is the overlap integral of electron wave functions in a graphite layer, a_0 is the lattice constant, d_{002} is the distance between graphite layers, $\hbar$ is the Plank's constant, L_{ef} is the effective mean free path of charge carriers, E_F is the Fermi energy, e is the electron charge. In the approximation of independence of all scattering mechanisms the effective mean free path of charge carriers takes the form

$$\frac{1}{L_{ef}} = \frac{1}{L_{ph}} + \frac{1}{L_b} + \frac{1}{L_{def}} + \frac{1}{L_{imp}}, \tag{2}$$

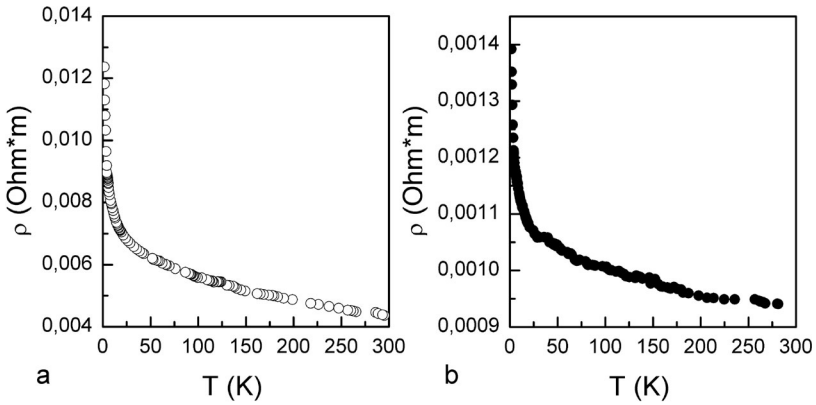

Figure 1 Temperature dependence of resistance for the pure MWCNT (a) and N-MWCNT samples (b).

where L_{ph}, L_b, L_{def}, and L_{imp} are the mean fee paths for the scattering of charge carries by phonons, crystalline boundaries, defects, and impurities, respectively. The temperature dependence of the specific electric resistance is determined by the temperature dependence of the charge-carrier density and of their mean free path. For MWCNT, as well as for other fine-crystalline graphite materials, for which a very small overlapping of the valence and conduction bands occurs, the density of free charge carriers practically does not change at temperatures up to 50 K. With regard to the temperature dependence of charge-carrier mean free path, it is determined by the temperature dependences of mean free paths for different scattering mechanisms. Apparently, among all the considered scattering mechanisms for MWCNT, in the first approximation the scattering by defects, crystallite boundaries and impurities are expected to be temperature independent. The scattering of charge carriers by phonons obviously depends on temperature. Furthermore, the effective mean free path of charge carriers is determined by the scattering mechanism, for which the mean free path is minimal. Let us assume that the mean free path for the scattering by phonons in MWCNT is of the same order as for the crystalline graphite ($L_{ph} \sim 200$ nm at $T = 273$ K [29]). Then, for the temperature-independent scattering mechanisms, the mean free paths are approximately equal to the size of crystallites in MWCNT. According to estimations from X-ray diffraction, the mean crystallite sizes are about 20 nm for pure MWCNT and about 18 nm for nitrated MWCNT. Hereby, the mean free path for the scattering by phonons is much larger than the corresponding values for the scattering by crystallite boundaries, defects and impurities. Thus, the main mechanism of the scattering of charge carriers in MWCNT is the temperature-independent scattering by crystallite boundaries. Both a small increase of the charge-carrier density with the growing temperature and a weak dependence of charge-carrier mobility upon temperature cause a small decrease of electric resistance with temperature, which in fact is observed experimentally at high temperatures. According to classical scattering mechanisms, at low temperatures the electrical resistance either does not depend on temperature or increases negligibly with temperature decreasing. However, the experimental dependence $\rho(T)$ shows an anomalous resistance increase with decreasing temperature that cannot be explained in the framework of the classical theory of electrical conductivity. Such an anomalous temperature dependence of the WNT conductivity may be related with manifestation of the effects of weak localization and electron–electron interactions, which take place in weakly disordered systems. For the reason that transport properties of nanotubes are similar to the properties of turbostratic graphite, the formulas for two-dimensional systems were used to describe quantum interference phenomena in MWCNT.

In the framework of the theory of weak localization and interaction of charge carriers, the electrical conductivity of the system can be written as [30–33]

$$\sigma(T) = \sigma_{cl}(T) + \Delta\sigma_q(T),$$
$$\Delta\sigma_q(T) = \Delta\sigma_{loc}(T) + \Delta\sigma_{el-el}(T), \quad (3)$$

where σ_{cl} is the classical conductivity, $\Delta\sigma_q$ is the contribution to the conductivity related to quantum effects, being the sum of contribution due to the weak localization effect, $\Delta\sigma_{loc}$, and the contribution due to the effect of charge-carrier interaction, $\Delta\sigma_{el-el}$. In the two-dimensional case the contribution to the conductivity resulting from weak localization has the form [34]

$$\Delta\sigma_{2loc}(T) = \frac{e^2}{2\pi^2\hbar}\alpha \ln\left(\frac{\tau_0}{\tau_\varphi}\right),$$

where

$$\tau_\varphi = A^* T^{-p}, \quad (4)$$

and the contribution to conductivity resulting from the effect of charge carriers interaction $\Delta\sigma_{2el-el}$ is:

$$\Delta\sigma_{2el-el}(T) = \frac{e^2}{2\pi^2\hbar}\gamma \ln\left(\frac{k_B T\tau_0}{\hbar}\right). \quad (5)$$

Here, τ_0 is the charge-carrier relaxation time for different scattering mechanisms, τ_φ is the phase relaxation time, A^*

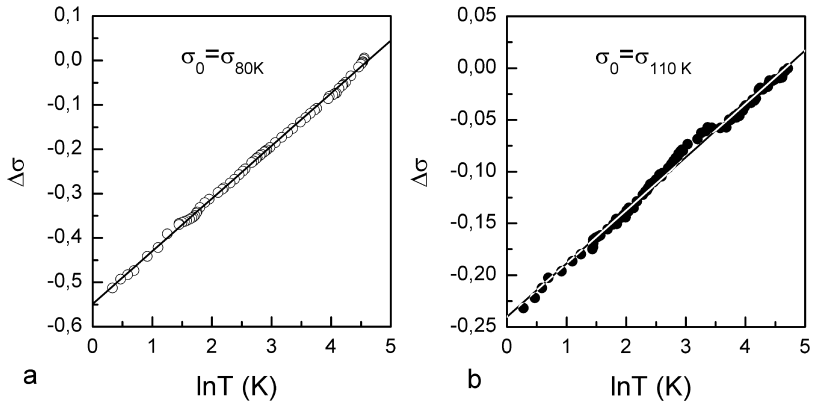

Figure 2 Dependence of $\Delta\sigma$ versus $\ln(T)$ for pure MWCNT (a) and N-MWCNT (b) samples.

and p are coefficients, a is a numerical coefficient, which depends on the relation between τ_0 and τ_φ; γ is the numerical coefficient characterizing the screening of charge carriers [35, 36].

By taking into account Eqs. (3)–(5) for the correction for two-dimensional conductivity, we obtain

$$\Delta\sigma_{2q}(T) = \Delta\sigma_{2loc}(T) + \Delta\sigma_{2el-el}(T) = \frac{e^2}{2\pi^2\hbar}\left[(ap+\gamma)\ln(T) + \gamma\ln\left(\frac{2\pi k_B T\tau_0}{\hbar}\right) + a\ln\left(\frac{\tau_0}{A^*}\right)\right], \quad (6)$$

or in the simplified form

$$\Delta\sigma_{2q}(T) = K\ln(T) + E \quad (7)$$

where

$$K = \frac{e^2}{2\pi^2\hbar}(ap+\gamma);$$

$$E = \frac{e^2}{2\pi^2\hbar}\left[\gamma\ln\left(\frac{2\pi k_B T\tau_0}{\hbar}\right) + a\ln\left(\frac{\tau_0}{A^*}\right)\right].$$

Thus, for the two-dimensional system the contributions to conductivity, which are related to the effects of weak localization and charge-carrier interaction, are proportional to $\ln(T)$.

In Fig. 2, the dependence $\Delta\sigma(T) = (\sigma(T)/\sigma_0 - 1)$ versus $\ln(T)$ is shown, where σ_0 is the conductivity at the temperature for which the dependence $\Delta\sigma(T)$ deviates from the linear one. As can be seen in Fig. 2, the linear dependence $\Delta\sigma$ versus $\ln(T)$ is observed for both the pure and nitrated MWCNT. Note that for the nitrated MWCNT the slope coefficient of the straight line is half that for the MWCNT before nitrogen doping. Thereby, the obtained linear dependencies $\Delta\sigma$ versus $\ln(T)$ indicate a possible manifestation in MWCNT the effects of weak localization and electron–electron interaction for the two-dimensional case.

In Fig. 3, the experimental dependences of electrical conductivity on the magnetic field are shown for the pure MWCNTs (Fig. 3a) and N-doped MWCNT (Fig. 3b) samples. As can be seen in Fig. 3a, the magnetoresistance is negative for pure MWCNT over the entire range of temperatures 1.6–100.3 K and magnetic fields, and the value of $\Delta\rho/\rho$ changes from –4.3 to –2.8% at the maximum value of magnetic induction. Figure 3b shows the experimentally obtained dependence of the magnetoresistance for the N-doped MWCNT samples in the temperature range 1.6–70.2 K. At 1.6 K, the magnetoresistance for N-doped MWCNT is –2.7% at the maximum value of magnetic induction, whereas with increasing temperature the magnetoresistance is reduced at the maximum value of magnetic induction. Moreover, the magnitude of magnetoresistance decreases under the modification of MWCNT with nitrogen (see Fig. 3b).

Let us analyze the obtained experimental data on the resistance changes in magnetic field in the framework of the theories of weak localization and electron–electron interactions for the two-dimensional case. Taking into account the quantum effects, the contribution to conductivity in the magnetic field can be written in the form [30, 36]

$$\Delta\sigma_q(B) = \Delta\sigma_{loc}(B) + \Delta\sigma_{el-el}(B), \quad (8)$$

where $\Delta\sigma_{loc}(B)$ is the contribution to conductivity in magnetic field due to the weak localization, $\Delta\sigma_{el-el}(B)$ is the contribution to conductivity due to the interaction of electrons.

The contribution to conductivity in the magnetic field, which is related to the two-dimensional effect of weak localization, is determined as [30]

$$\Delta\sigma_{loc}(B) = \frac{e^2}{2\pi^2\hbar}Y\left(\frac{4eDB\tau_\varphi}{\hbar}\right), \quad (9)$$

$$Y(x) \simeq \begin{cases} x^2/24, & \text{for} \quad x \ll 1 \\ \ln(x), & \text{for} \quad x \gg 1 \end{cases} \quad (10)$$

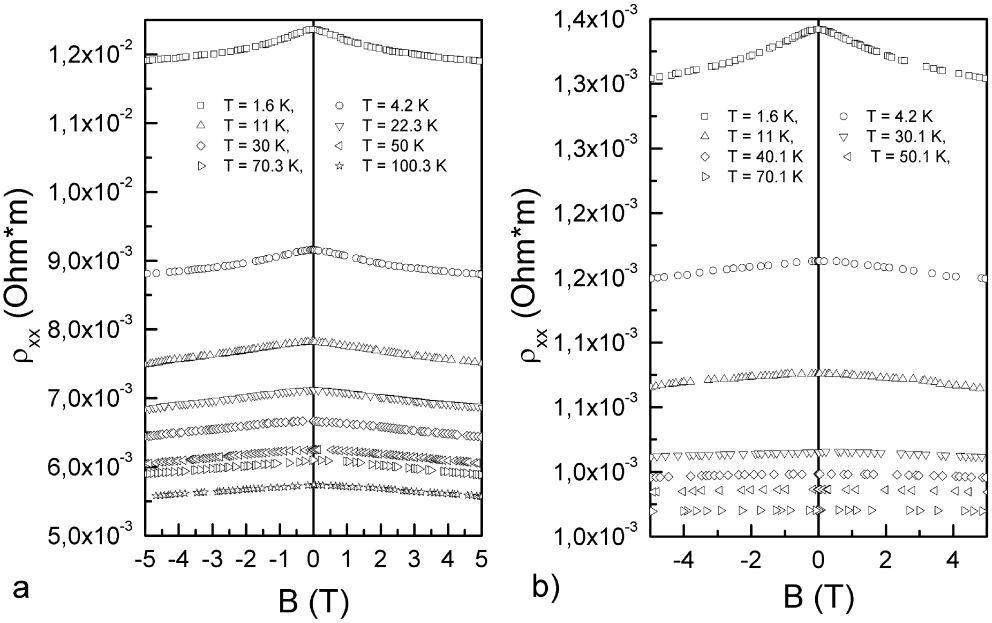

Figure 3 Magnetic field dependence of resistance for pure MWCNT (a) and N-MWCNT (b) samples.

where $\Delta\sigma_{\rm loc}(B) = \sigma_{\rm loc}(B) - \sigma_{\rm loc}(B = 0)$, D is a diffusion coefficient. The characteristic field is determined by the formula:

$$B_{\rm loc} \sim \frac{\hbar}{4eD\tau_\varphi}. \tag{11}$$

The contribution to the two-dimensional conductivity in magnetic field is caused by the effect of the electron–electron interaction and appears as:

$$\Delta\sigma_{\rm el-el}(B) = \frac{e^2}{2\pi^2\hbar} g\,(T, B)\, f_2\left(\frac{2eDB}{\pi k_{\rm B}T}\right), \tag{12}$$

$$f_2(x) \simeq \begin{cases} 0.3x^2, & \text{for} \quad x \ll 1 \\ \ln(x), & \text{for} \quad x \gg 1 \end{cases} \tag{13}$$

where $g(T, B)$ is the parameter of electron–electron interaction. The characteristic field for this case is determined by the relation:

$$B_{\rm el-el} \sim \frac{\pi k_{\rm B}T}{2eD}. \tag{14}$$

Thus, for the two-dimensional system in case of small magnetic fields (which are lower than the characteristic field) both contributions to conductivity are proportional to the square of magnetic field, whereas at high fields the dependences of both contributions on magnetic field have a logarithmic character.

The reconstructed experimental dependences of magnetoresistance on magnetic field at low temperatures, $\Delta\sigma_{\rm q}(B) = (\sigma(B)/\sigma - 1)$ versus B are given in Fig. 4 for the samples of pure and N-doped MWCNT. As is seen in

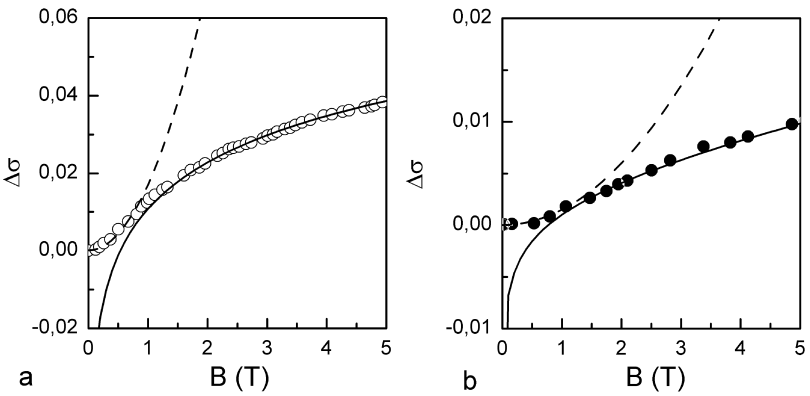

Figure 4 Magnetic field dependencies of $\Delta\sigma_{\rm q}(B)$ for pure MWCNT (a) and N-MWCNT (b) samples at 1.6 K. Dashed line is dependence $y_1 \sim a_1 B^2$, solid line is dependence $y_2 = b + a_2 \ln(B)$.

Table 1 Calculated values of some parameters for the investigated samples.

	MWCNT	N-MWCNT
L_T (nm)	20	18
D ($m^2\,s^{-1}$)	2.27×10^{-4}	2.02×10^{-4}
B_{el-el} (T)	2.5	3
p	0.98	1.2
E_F (eV)	0.006	0.1

Fig. 4, the experimental dependence $\Delta\sigma_q$ versus B for all given samples at low magnetic fields can be approximated by a square field dependence of $y_1 \sim a_1 B^2$ type, and at high magnetic fields by logarithmic dependence of $y_2 = b + a_2 \ln(B)$ type. Therefore, for the obtained experimental dependences of magnetoresistance, both for pure and N-doped MWCNT, the following relations take place: at low fields the contribution to conductivity in magnetic field is proportional to the square of the magnetic field, and at high magnetic fields it is proportional to a logarithm of the magnetic field.

The diffusion coefficient of charge carriers D for pure and N-doped MWCNT samples can be defined as:

$$D = \frac{L_T^2 k_B T}{\hbar}, \tag{15}$$

where L_T is the coherence length in conductor (i.e., the mean-free path of charge carriers for inelastic processes). The temperature dependence of $D(T)$ is determined by a temperature dependence of L_T. For the dominating phonon mechanism of charge-carrier scattering, L_T decreases with temperature, and obviously $D(T)$ decreases with increasing temperature. However, as is shown above, the special situation is observed for the studied MWCNT: the main mechanism of scattering of charge carriers is the scattering at boundaries of crystallites. In this case, L_T is determined by the sizes of the crystallites in the investigated MWCNT, and obviously the L_T does not depend on temperature. According to Eq. (15), this provides a growth of the diffusion coefficient with temperature. Taking into account the sizes of crystallites, which were estimated by X-ray diffraction for pure and N-doped MWCNT, the values of the diffusion coefficients at temperature of 1.6 K amount to 2.269×10^{-4} and $2.020 \times 10^{-4}\,m^2\,s^{-1}$ for pure and N-doped MWCNT samples, respectively (see Table 1).

For both systems, we can estimate the values of characteristic fields. In the case of electron–electron interaction of charge carriers, a value of the characteristic field can be determined by Eq. (14) taking into account Eq. (15):

$$B^*_{el-el} = \frac{\pi k_B T}{2eD} = \frac{\pi k_B T \hbar}{2eL_T^2 k_B T} = \frac{\pi\hbar}{2eL_T^2}. \tag{16}$$

By this means the characteristic field B_{el-el} does not depend on temperature, and is determined only by the sizes of the crystallites in the investigated material. The values of characteristic field B_{el-el} amount to ~2.5 T for pure MWCNT and ~3.0 T for N-doped MWCNT. Apparently from Fig. 4, for both pure and N-doped MWCNT the magnetic fields, where a deviation from square dependence of $y_1 \sim a_1 B^2$ was observed, are significantly smaller. Obviously, this is related to that the characteristic fields of localization are smaller, than that of interaction.

According to Eq. (11), the temperature dependence of the characteristic field of localization B_{loc} is determined by the temperature dependences of two parameters: the diffusion coefficient, which linearly grows with temperature, Eq. (15), and the time of the phase breaking τ_φ (time of phase relaxation), which decreases with temperature growth, in line with Eq. (4). For the two-dimensional system, the exponent p can gain values from 0.5 to 2 [37]. Let us take the logarithm of the expression for characteristic field in the case of weak localization, taking into account Eqs. (4) and (15):

$$\ln(B_{loc}) = \ln\left(\frac{\hbar^2}{4eL_T^2 k_B A^*}\right) + (p-1)\ln(T). \tag{17}$$

We can estimate the values of characteristic fields of localization B_{loc} from experimental data in Fig. 4 as magnetic fields at which the dependence $\Delta\sigma_q(B) = (\sigma(B)/\sigma_0 - 1)$ versus B deviates from the squared one.

In Fig. 5, the temperature dependences of the characteristic fields of localization B_{loc} versus T, as determined from experimental data, are given in logarithmic coordinates. From these dependences, with use of Eq. (17), the values p and A^* for pure and N-doped MWCNT are estimated and given in Table 1.

As appears from Table 1, for pure MWCNT the value of p amounts to 0.98. Therefore, in good approximation, it is possible to consider that for pure MWCNT the dependence $\tau_\varphi = A^*/T$ occurs. For N-doped MWCNT $p = 1.20$, that is, the dependence of the phase-relaxation time on temperature is more pronounced. As for the A^* factor, its values for pure and N-doped MWCNT do not differ substantially. Thus, from the experimental data on the behavior of conductivity in a magnetic field, the temperature dependences of the phase-relaxation time for the wave functions of charge carriers τ_φ were obtained for pure and N-doped MWCNT samples.

The relative contribution to the two-dimensional conductivity resulting from the manifestation of weak localization effects and interaction in magnetic field, which is less than a characteristic field of localization, can be written as:

$$\Delta\sigma = \frac{2\sqrt{3}e^2 D^2 \gamma_0 a_0}{\pi E_F L_T}\left(\frac{\tau_\varphi^2}{6\hbar} + \frac{0.3G}{\pi^2 k_B^2 T^2}\right) B^2. \tag{18}$$

Let us consider in detail the coefficient a at B^2 which we will designate as a_{1CNT} for pure MWCNT and a_{1N} for N-doped MWCNT. In the expression for the coefficient at B^2, we substitute in an explicit form the diffusion coefficient D and the relaxation time τ_φ for the wave function. For the pure

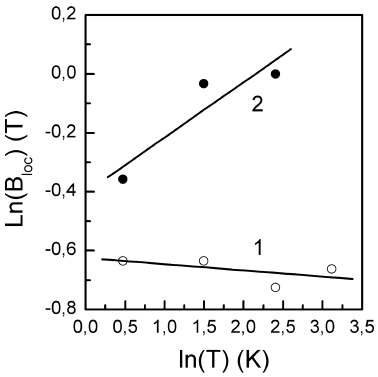

Figure 5 Dependence of $\ln(B_{\rm loc})$ versus $\ln(T)$: (1) pure MWCNT; (2) N-MWCNT.

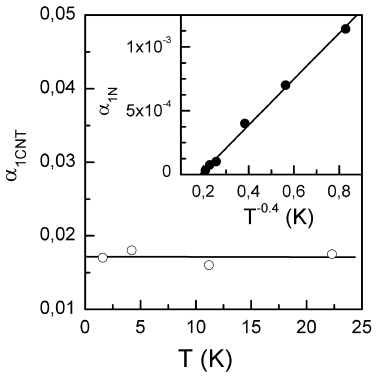

Figure 6 Temperature dependences of coefficient $a_{1\rm N}(T)$ for pure MWCNT and N-MWCNT (inset).

MWCNT, this expression takes the form:

$$a_{1\rm CNT} = \frac{2\sqrt{3}e^2L_T^3k_{\rm B}^2\gamma_0 a_0}{\pi E_{\rm F}\hbar^2}\left(\frac{(A^*)^2}{6\hbar^2} + \frac{0.3G}{\pi^2k_{\rm B}^2}\right). \tag{19}$$

This means that the coefficient of B^2 in Eq. (18) does not depend on temperature. From the analysis of experimental data in Fig. 6, it follows that in the range of temperatures 1.6–22.3 K the temperature dependence of the coefficient at B^2 in Eq. (18) is very weak indeed. In expression (19) for the case of pure MWCNT there are two unknown parameters: the energy of the Fermi level $E_{\rm F}$ and a constant G, which is much less than 1 in the case of small magnetic fields, as was shown in Ref. [35]. According to our calculations, with reduction of parameter G, the energy $E_{\rm F}$ asymptotically comes to the value of about 0.01 eV, which can be taken for pure MWCNT.

Next, we will analyze the temperature dependence of $a_{1\rm N}(T)$ for N-doped MWCNT. As shown above, for these MWCNT the temperature dependence of the phase relaxation time τ_φ can be written as $\tau_\varphi = A^*/T^{1/2}$. If we substitute this for the phase-relaxation time in Eq. (17), we will obtain the following expression:

$$\begin{aligned} a_{1\rm N}(T) &= \frac{2\sqrt{3}e^2L_T^3k_{\rm B}^2\gamma_0 a_0}{\pi E_{\rm F}\hbar^2}\left[\frac{(A^*)^2}{6\hbar^2T^{0.4}} + \frac{0.3G}{\pi^2k_{\rm B}^2}\right] \\ &= K_1T^{-0.4} + K_2, \end{aligned} \tag{20}$$

where

$$K_1 = \frac{2\sqrt{3}e^2L_T^3k_{\rm B}^2\gamma_0 a_0\,(A^*)^2}{6\pi E_{\rm F}\hbar^4},$$

$$K_2 = \frac{2\sqrt{3}e^2L_T^3\gamma_0 a_0 0.3G}{\pi^3 E_{\rm F}\hbar^2}.$$

Therefore, in the case of N-doped MWCNT, the experimentally obtained coefficients $a_{1\rm N}(T)$ at B^2 have to depend linearly on $T^{-0.4}$. Apparently, the linear dependence of $a_{1\rm N}(T)$ versus $T^{-0.4}$ can be clearly seen in Fig. 6. The values K_1 and K_2 were determined from the experimental dependence $a_{1\rm N}(T)$ versus $T^{-0.4}$ and allowed to estimate the energy of Fermi level and the constant G, which appeared to be: $E_{\rm F} = 0.1$ eV, $G = 2.0 \times 10^{-2}$. Thus, nitrogen doping of MWCNT leads to $E_{\rm F}$ growth by 10 times in comparison with pure MWCNT. This change of $E_{\rm F}$ is presumably related with a growth of charge-carrier density under nitrogen doping of MWCNT. This is also in agreement with observed reduction of the specific resistance of nitrated MWCNT.

The relative contribution to two-dimensional conductivity in the case of strong magnetic fields, that is $B > B_{\rm el-el}$, takes the form:

$$\begin{aligned} \Delta\sigma = \frac{\sqrt{3}\gamma_0 a_0}{2\pi E_{\rm F}L_T}\Bigg[&\ln\left(\frac{4eDB\tau_\varphi}{\hbar}\right) \\ &+ G\ln\left(\frac{2eD}{\pi k_{\rm B}T}\right) + (1+G)\ln(B)\Bigg]. \end{aligned} \tag{21}$$

At a constant temperature the dependence Eq. (21) can be written in the form of $\Delta\sigma = b + a\,(1 + G(B))\ln(B)$. Apparently from Fig. 4, at high magnetic fields such a dependence of $\Delta\sigma(B)$ is really observed experimentally. However, it is rather difficult to obtain any quantitative estimates in this interval of magnetic fields, since for strong magnetic fields the constant G depends in a complicated way on temperature and magnetic field:

$$\frac{1}{G} = \frac{1}{\lambda} + \ln\left(\frac{c\eta}{eBD}\right),$$

$$\frac{1}{G} = \frac{1}{\lambda} + \ln\left(\frac{\gamma\eta}{\pi K_{\rm B}T}\right),$$

where the numerical values of the constants λ and η are basically unknown.

4 Conclusions The investigations of resistance and magnetoresistance of pure MWCNT and N-doped MWCNT samples have revealed the influence of nitrogen doping on the electronic structure of MWCNT. It is established that nitrogen doping of MWCNT leads to growth of the density of delocalized charge carriers in MWCNT, which in turn leads

to a reduction of the specific resistance of N-doped MWCNT. This is also confirmed by our estimations of the change of the Fermi-level energy under nitrogen doping. As shown by the calculations, under nitrogen doping the Fermi level is shifted into the valence band, and the value of the Fermi-level energy increases by 10 times. The estimations of the diffusion coefficient are carried out for pure and nitrated MWCNT. It is revealed that for pure and N-doped MWCNT the manifestation of the effects of weak localization and electron–electron interactions takes place in the kinetic properties of charge carriers at low temperatures. This results in abnormal temperature and field dependences of resistance, in particular, in the manifestation of a negative magnetoresistance. On the basis of the conducted investigations, the explicit type of temperature dependence of the phase relaxation time of the wave function is established for the pure and nitrated MWCNT.

Acknowledgement This work was partly supported by the SPS NATO grant N 984243.

References

[1] A. Cottet, T. Kontos, S. Sahoo, H. T. Man, M. S. Cho, W. Belzig, C. Bruder, A. F. Morpurgo, and C. Schönenberger, Semicond. Sci. Technol. **21**, S78 (2006).
[2] L. Y. Matzui, I. V. Ovsienko, T. A. Len, Y. I. Prylutskyy, and P. Scharff, Fullerenes Nanotubes Carbon Nanostruct. **13**, 259 (2005).
[3] I. Ovsienko, T. Len, L. Matzui, Y. Prylutskyy, P. Eklund, F. Normand, U. Ritter, and P. Scharff, Physica E **37**, 78 (2007).
[4] G. E. Grechnev, V. A. Desnenko, A. V. Fedorchenko, A. S. Panfilov, Y. A. Kolesnichenko, L. Y. Matzui, M. I. Grybova, Y. I. Prylutskyy, U. Ritter, and P. Scharff, Low Temp. Phys. **36**, 1086 (2010).
[5] U. Ritter, P. Scharff, G. E. Grechnev, V. A. Desnenko, A. V. Fedorchenko, A. S. Panlov, Y. I. Prylutskyy, and Y. Kolesnichenko, Carbon **49**, 4443 (2011).
[6] R. Czerw, M. Terrones, J. C. Charlier, X. Blase, B. Foley, R. Kamalakaran, N. Grobert, H. Terrones, D. Tekleab, P. M. Ajayan, W. Blau, M. Rühle, and D. L. Carroll, Nano Lett. **1**, 457 (2001).
[7] A. Nevidomskyy, G. Csanyi, and M. Payne, Phys. Rev. Lett. **91**, 105502 (2002).
[8] P. Nemes-Incze, N. Dároczi, Z. Sárközi, K. K. A. Koós, O. Iprigan, Z. E. Horváth, A. Darabont, and L. P. Bipó, J. Optoelectron. Adv. Mater. **9**, 1525 (2007).
[9] S. van Dommele, A. Romero-Izquirdo, R. Brydson, K. P. de Jong, and J. Bitter, Carbon **46**, 138 (2008).
[10] X. Li, Y. Liu, L. Fu, L. Cao, D. Wei, and Y. Wang, Carbon **46**, 255 (2008).
[11] L. Bulusheva, A. Okotrub, A. Kudashov, Y. Shubin, E. Shlyakhova, N. Yudanov, E. Pazhetnov, A. Boronin, and D. Vyalikh, Carbon **46**, 864 (2008).
[12] A. A. Koós, M. Dowling, K. Jurkschat, A. Crossley, and N. Grobert, Carbon **47**, 30 (2009).
[13] H. Mousavi and R. Moradian, Solid State Sci. **3**, 1459 (2011).
[14] H. Khalfoun and L. H. Ph. Lambin, Phys. Rev. B **89**, 045407 (2014).
[15] S. H. Lim, H. I. Elim, X. Y. Gao, A. T. S. Wee, W. Ji, J. Y. Lee, and J. Lin, Phys. Rev. B **74**, 045402 (2006).
[16] Y. M. Choi, D. S. Lee, R. Czerw, P. W. Chiu, N. Grobert, M. Terrones, M. Reyes-Reyes, H. Terrones, J. C. Charlier, P. M. Ajayan, S. Roth, D. L. Carroll, and Y. W. Park, Nano Lett. **3**, 839 (2003).
[17] M. Salvato, M. Lucci, I. Ottaviani, M. Cirillo, E. Tamburri, I. Cianchetta, V. Guglielmotti, S. Orlanducci, M. L. Terranova, and M. Pasquali, Phys. Rev. B **84**, 233406 (2011).
[18] S. Ahn, Y. Kim, Y. Nam, H. Yoo, J. Park, Y. Park, Z. Wang, Z. Shi, and Z. Jin, Phys. Rev. B **80**, 165426 (2001).
[19] S. Enouz, J. L. Bantignies, M. R. Babaa, L. Alvarez, P. Parent, F. L. Normand, O. Stéphan, P. Poncharal, A. Loiseau, and B. P. Doyle, J. Nanosci. Nanotechnol. **7**, 3524 (2007).
[20] C. Deck and K. Vecchio, J. Phys. Chem. B **12353**, 109 (205).
[21] N. Tran, M. Wilson, A. Milev, J. Bartlett, R. Lamb, D. Martin, and G. Kannangara, Adv. Colloid Interface Sci. **145**, 23 (2009).
[22] A. A. Koós, F. Dillon, E. A. Obraztsova, A. Crossley, and N. Grobert, Carbon **48**, 3033 (2010).
[23] O. Mykhailenko, Y. Prylutskyy, and L. Kondratenko, Phys. Met. Adv. Technol. **32**, 1477 (2010).
[24] U. Ritter, N. G. Tsierkezos, Y. I. Prylutskyy, L. Y. Matzui, V. O. Gubanov, M. O. D. M. M. Bily, and M. O. Davydenko, J. Mater. Sci. **47**, 2390 (2012).
[25] G. E. Grechnev, V. A. Desnenko, A. V. Fedorchenko, A. S. Panfilov, Y. A. Kolesnichenko, S. V. Khrapatiy, Y. I. Prylutskyy, L. Matzui, U. Ritter, and P. Scharff, Mater.wiss. Werkst.tech. **44**, 136 (2013).
[26] P. Szroeder, N. G. Tsierkezos, P. Scharff, and U. Ritter, Carbon **48**, 4489 (2010).
[27] I. V. Ovsienko, T. A. Len, L. Y. Matzui, Y. I. Prylutskyy, U. Ritter, P. Scharff, F. L. Normand, and P. Eklund, Mol. Cryst. Liq. Cryst. **468**, 289 (2007).
[28] P. Wallace, Phys. Rev. **71**, 622 (1947).
[29] S. Shulepov, Physics of Carbon-Graphite Materials (in Russian) (Metallurgy, Moscow, 1972).
[30] B. Altshuler, D. Khmelnitzkii, A. Larkin, and P. Lee, Phys. Rev. B **22**, 5142 (1980).
[31] B. Altshuler and A. Aronov, Solid State Commun. **54**, 713 (1985).
[32] Y. Koike, S. Morita, T. Nakanomyo, and T. Fukase, J. Phys. Soc. Jpn. **54**, 713 (1985).
[33] L. Langer, V. Bayot, E. Grivei, J. P. Issi, J. P. Heremans, C. H. Olk, L. Stockman, C. V. Haesendonck, and Y. Bruynseraede, Phys. Rev. Lett. **76**, 479 (1996).
[34] L. Piraux, V. Bayot, J. P. Michenaud, and J. P. Issi, Phys. Scr. **37**, 942 (1988).
[35] B. Altshuler, A. Aronov, A. Larkin, and D. Khmelnitsky, Sov. Phys. JETP **54**, 441 (1981).
[36] P. Lee and T. Ramakrishman, Rev. Mod. Phys. **57**, 287 (1985).
[37] B. Altshuler, A. Aronov, M. Gershenson, and Y. Sharvin, in: Soviet Science Review A, Vol. 9 (Harwood Academic Publisher Gmbh, Chur, Switzerland, 1987).